

REPORT DOCUMENTATION PAGE			Form Approved OMB No. 0704-0188		
Public reporting burden for this collection of information is estimated to average 1 hour per response, including the time for reviewing instructions, searching existing data sources, gathering and maintaining the data needed, and completing and reviewing this collection of information. Send comments regarding this burden estimate or any other aspect of this collection of information, including suggestions for reducing this burden to Department of Defense, Washington Headquarters Services, Directorate for Information Operations and Reports (0704-0188), 1215 Jefferson Davis Highway, Suite 1204, Arlington, VA 22202-4302. Respondents should be aware that notwithstanding any other provision of law, no person shall be subject to any penalty for failing to comply with a collection of information if it does not display a currently valid OMB control number. <b>PLEASE DO NOT RETURN YOUR FORM TO THE ABOVE ADDRESS.</b>					
1. REPORT DATE (DD-MM-YYYY) 14-11-2005		2. REPORT TYPE Journal Article		3. DATES COVERED (From - To)	
4. TITLE AND SUBTITLE  Structural Characterization of POSS Siloxane Dimer and Trimer (PREPRINT)		5a. CONTRACT NUMBER			
		5b. GRANT NUMBER			
		5c. PROGRAM ELEMENT NUMBER			
6. AUTHOR(S) Timothy Haddad (ERC); Ashwani Vij (AFRL/PRSP); Stan Anderson & Connie Mitchell (Westmont College); Joseph Schwab (Hybrid Plastics); Mike Bowers (UCSB)		5d. PROJECT NUMBER 23030521			
		5e. TASK NUMBER			
		5f. WORK UNIT NUMBER			
7. PERFORMING ORGANIZATION NAME(S) AND ADDRESS(ES)  Air Force Research Laboratory (AFMC) AFRL/PRSM 9 Antares Road Edwards AFB CA 93524-7401		8. PERFORMING ORGANIZATION REPORT NUMBER  AFRL-PR-ED-JA-2005-452			
9. SPONSORING / MONITORING AGENCY NAME(S) AND ADDRESS(ES)  Air Force Research Laboratory (AFMC) AFRL/PRS 5 Pollux Drive Edwards AFB CA 93524-7048		10. SPONSOR/MONITOR'S ACRONYM(S)			
		11. SPONSOR/MONITOR'S NUMBER(S) AFRL-PR-ED-JA-2005-452			
12. DISTRIBUTION / AVAILABILITY STATEMENT  Approved for public release; distribution unlimited (AFRL-ERS-PAS-2005-289)					
13. SUPPLEMENTARY NOTES Submitted for publication in Chemistry of Materials					
14. ABSTRACT Ion mobility and molecular modeling methods were used to examine the gas phase conformational properties of POSS (Polyhedral Oligomeric Silsesquioxanes) siloxane oligomers. MALDI generated the sodiated dimers (C <sub>7</sub> T <sub>8</sub> ) <sub>2</sub> O·Na <sup>+</sup> and (C <sub>7</sub> T <sub>8</sub> ) <sub>2</sub> O·Na <sup>+</sup> , and the trimer ion [C <sub>7</sub> T <sub>8</sub> O-Cy <sub>8</sub> Si <sub>8</sub> O <sub>11</sub> -OCy <sub>7</sub> T <sub>8</sub> ] Na <sup>+</sup> (T = SiO <sub>1.5</sub> , Cy = cyclohexyl, and Cp = cyclopentyl); their collision cross-sections were measured in helium using ion mobility based methods. Experimental results are consistent with one observed conformer for each of the dimers, and the exo-exo isomer for the trimer (formed by retention of configuration at silicon during synthesis). For the cyclopentyl dimer, theory predicts two separate conformer families based on whether the substituents on the POSS cages are staggered ( $\sigma_{\text{calc}} = 357 \text{ \AA}^2$ ) or eclipsed ( $\sigma_{\text{calc}} = 365 \text{ \AA}^2$ ); experiment fits the staggered conformation best ( $\sigma_{\text{expt}} = 355 \text{ \AA}^2$ ). For the cyclohexyl dimer, on the other hand, folding of the Cy groups seems to be important: ( $\sigma_{\text{expt}} = 402 \text{ \AA}^2$ vs unfolded $\sigma_{\text{calc}} = 421 \text{ \AA}^2$ or folded $\sigma_{\text{calc}} = 407 \text{ \AA}^2$ ). Similar to the Cy dimer, for the trimer theory indicates that a low energy exo-exo family of structures fits the experimental cross-section ( $\sigma_{\text{expt}} = 557 \text{ \AA}^2$ ) only if several Cy-groups are folded ( $\sigma_{\text{calc}} = 557 \text{ \AA}^2$ ) as compared to unfolded structures (avg. $\sigma_{\text{calc}} = 570 \text{ \AA}^2$ ). Modeling shows the non-bonded interactions of the capping Cp and Cy groups stabilize POSS cage packing leading to compact structures being lowest in energy. Modeling also suggests that two POSS cages bonded together by a single oxygen atom gives a benchmark 8.3 – 8.5 Å cage-cage center distance which may be used to evaluate cage packing in other POSS oligomers.					
15. SUBJECT TERMS					
16. SECURITY CLASSIFICATION OF:			17. LIMITATION OF ABSTRACT	18. NUMBER OF PAGES	19a. NAME OF RESPONSIBLE PERSON
a. REPORT	b. ABSTRACT	c. THIS PAGE			Dr. Joseph M. Mabry
Unclassified	Unclassified	Unclassified	A	29	19b. TELEPHONE NUMBER (include area code) N/A

# Structural Characterization of POSS Siloxane Dimer and Trimer (Preprint)

*Stanley E. Anderson<sup>a</sup>, Connie Mitchell, Timothy S. Haddad<sup>b</sup>, Ashwani Vij<sup>c</sup>, Joseph J. Schwab<sup>d</sup>, and  
Michael T. Bowers\**

*Department of Chemistry & Biochemistry, University of California, Santa Barbara, CA 93106*

*<sup>a</sup>Department of Chemistry, Westmont College, Santa Barbara, CA 93108*

*<sup>b</sup>ERC Inc., <sup>c</sup>Air Force Research Laboratory, 10 East Saturn Boulevard, Building 8451, Edwards AFB,  
CA 93524-7680*

*<sup>d</sup>Hybrid Plastics, Inc., 18237 Mt. Baldy Circle, Fountain Valley, CA, 92708*

## RECEIVED DATE

TITLE RUNNING HEAD    Structure of Polyhedral Oligomeric Silsesquioxane Siloxane (POSS)  
Oligomers

## CORRESPONDING AUTHOR FOOTNOTE

\* Corresponding author: Phone: 805-893-2893. Email: bowers@chem.ucsb.edu

Distribution A. Approved for public release, distribution unlimited.

## Abstract

Ion mobility and molecular modeling methods were used to examine the gas phase conformational properties of POSS (Polyhedral Oligomeric Silsesquioxanes) siloxane oligomers. MALDI generated the sodiated dimers  $(\text{Cy}_7\text{T}_8)_2\text{O}\cdot\text{Na}^+$  and  $(\text{Cp}_7\text{T}_8)_2\text{O}\cdot\text{Na}^+$ , and the trimer ion  $[\text{Cy}_7\text{T}_8\text{O}-\text{Cy}_8\text{Si}_8\text{O}_{11}-\text{OCy}_7\text{T}_8] \text{Na}^+$  ( $\text{T} = \text{SiO}_{1.5}$ ,  $\text{Cy} = \text{cyclohexyl}$ , and  $\text{Cp} = \text{cyclopentyl}$ ); their collision cross-sections were measured in helium using ion mobility based methods. Experimental results are consistent with one observed conformer for each of the dimers, and the exo-exo isomer for the trimer (formed by retention of configuration at silicon during synthesis). For the cyclopentyl dimer, theory predicts two separate conformer families based on whether the substituents on the POSS cages are staggered ( $\sigma_{\text{calc}} = 357 \text{ \AA}^2$ ) or eclipsed ( $\sigma_{\text{calc}} = 365 \text{ \AA}^2$ ); experiment fits the staggered conformation best ( $\sigma_{\text{expt}} = 355 \text{ \AA}^2$ ). For the cyclohexyl dimer, on the other hand, folding of the Cy groups seems to be important: ( $\sigma_{\text{expt}} = 402 \text{ \AA}^2$  vs unfolded  $\sigma_{\text{calc}} = 421 \text{ \AA}^2$  or folded  $\sigma_{\text{calc}} = 407 \text{ \AA}^2$ ). Similar to the Cy dimer, for the trimer theory indicates that a low energy exo-exo family of structures fits the experimental cross-section ( $\sigma_{\text{expt}} = 557 \text{ \AA}^2$ ) only if several Cy-groups are folded ( $\sigma_{\text{calc}} = 557 \text{ \AA}^2$ ) as compared to unfolded structures (avg.  $\sigma_{\text{calc}} = 570 \text{ \AA}^2$ ). Modeling shows the non-bonded interactions of the capping Cp and Cy groups stabilize POSS cage packing leading to compact structures being lowest in energy. Modeling also suggests that two POSS cages bonded together by a single oxygen atom gives a benchmark 8.3 – 8.5 Å cage-cage center distance which may be used to evaluate cage packing in other POSS oligomers. X-ray crystal structures at 100K and 298K for  $(\text{Cy}_7\text{T}_8)_2\text{O}$  were carried out which show that solid state cage-cage intermolecular distances are perfectly consistent with the modeled POSS-PMA dimer and trimer structures. At room temperature there is considerable unresolved disorder of the cyclohexyl R-groups in the x-ray structure due to rapid boat-chair interconversion.

**KEYWORDS** POSS, Polyhedral oligomeric silsesquioxane (POSS), POSS siloxane, ion mobility, hybrid inorganic/organic

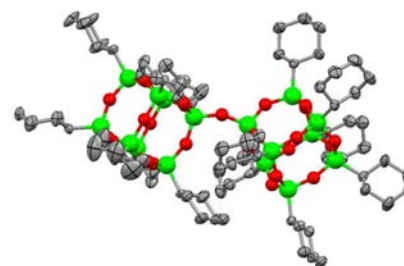
---

Stanley E. Anderson, Connie Mitchell,  
Timothy S. Haddad, Ashwani Vij, Joseph  
J. Schwab and Michael T. Bowers\*

*Chem. Mater.* **xxxx**, *xx*, xxxx

POSS Siloxane Oligomers Studies Using  
Ion Mobility Mass Spectrometry and  
Molecular Mechanics

The 100 K x-ray crystal structure of the  $(\text{Cy}_7\text{T}_8)_2\text{O}$  dimer. The experimental ion mobility measured collision cross-section was  $402 \text{ \AA}^2$ , compared to the modeled theoretical cross-section  $407 \text{ \AA}^2$ . For comparison, an x-ray cross-section of  $410 \text{ \AA}^2$  was calculated from x-ray coordinates.



---

## Introduction

The ability to enhance properties of materials for increased performance and environmental robustness is the focus of much current research. One approach to developing better materials is to create inorganic-organic composite materials in which inorganic building blocks are incorporated into organic polymers. Polyhedral Oligomeric Silsesquioxanes (POSS) are one type of hybrid inorganic/organic material of the form  $(\text{RSiO}_{3/2})_n$ , or  $\text{R}_n\text{T}_n$ , where organic substituents are attached to a silicon-oxygen cage.<sup>1</sup> The most common POSS cage is the  $\text{T}_8$  (a molecule with a cubic array of silicon atoms with bridging oxygen atoms and with 8 R groups to the silicon atoms at the vertexes of the cube). Other cages with well-defined geometries include  $n = 6, 10, 12, 14, 16$  and  $18$ .<sup>2,3</sup> By incorporating these Si-O cages into organic polymers, properties superior to the organic material alone are realized, offering exciting possibilities for the development of new materials.<sup>4-9</sup>

How the cage structures affect the polymer to which they are attached depends upon both the polymer type and the POSS used. Numerous papers suggest that POSS groups can undergo self-assembly/association to form POSS-rich domains that strongly affect polymer properties.<sup>10-21</sup> This association has been observed both by X-ray scattering and transmission electron microscopy. A recent

paper terms this a “bottom-up” approach to nanocomposite formation, where the POSS aggregate together to form rafts and sheets within a polymer matrix.<sup>20</sup>

In recent work, it was suggested that cage aggregation effects in POSS methacrylate oligomers appear to be important in determining the structure of these species.<sup>22</sup> The POSS cages seem to interact via non-bonded interactions and they are not merely space-filling entities. The tethered cages do not maximize their distances from each other, but rather tend to show a clustering effect. In order to further investigate this phenomena we decided to investigate the siloxane oligomers shown in Schemes 1 and 2 in which POSS cages were held together covalently by bridging oxygen linkages. The cage-cage center-to-center distance should be minimal in the siloxane system and provide a distance benchmark for cage separation in systems like the PMA oligomers where close approach of POSS cages must arise from cage interactions involving van der Waals non-bonded interactions of the R groups.

There are a few papers on POSS siloxanes demonstrating that such materials can be synthesized and showing their thermal and mechanical characteristics.<sup>23-25</sup> A primary observation is that the POSS group acts something like a hard segment to reinforce the rubbery siloxane material and raise its characteristic glass transition. Once again, the aggregation of the POSS appears to be responsible for the property changes.<sup>25</sup> There are recent theoretical papers<sup>26,27</sup> that demonstrate POSS aggregation when tethered or blended into polydimethylsiloxane.

Attempts to model siloxanes<sup>28-30</sup> are not new. Sun and Rigby<sup>31</sup> were the first to develop a comprehensive force field that was applied to simulations of siloxane molecular crystals, liquids and isolated molecules. Reasonable results were obtained for polydimethylsiloxane and polydiphenylsiloxane in the solid state, reproducing experimental data such as density and unit cell parameters and modeling gas phase geometries. DFT molecular orbital calculations on POSS systems are also well known and have been used to study the geometry and electronic structure of T<sub>8</sub> systems with simple R-groups such as H, methyl, and phenyl.<sup>32-35</sup>

## Experimental

### *Synthesis and Isolation of POSS siloxanes*

THF was dried over sodium benzophenone and vacuum transferred prior to use.  $\text{SiCl}_4$  (Geleste) was degassed and vacuum transferred prior to use. Butyllithium (Aldrich) was used as received as were the cyclohexyl and cyclopentylPOSS trisilanols,  $\text{R}_7[\text{Si}_7\text{O}_9](\text{OH})_3$  and monosilanols,  $\text{R}_7[\text{Si}_7\text{O}_{12}](\text{OH})$  (Hybrid Plastics).  $\text{Cy}_8\text{Si}_8\text{O}_{11}(\text{OH}_2)_2$  was synthesized by the literature procedure.<sup>36</sup> All NMR spectra were collected on either a Bruker 300 or 400 MHz instrument and obtained from  $\text{CDCl}_3$  solutions.  $^1\text{H}$ ,  $^{13}\text{C}$  and  $^{29}\text{Si}$  NMR spectra (reported in ppm using the  $\delta$  scale) were referenced to residual  $\text{CHCl}_3$  at 7.26 ppm, to  $\text{CDCl}_3$  at 77.0 ppm, and to external  $\text{SiMe}_4$  at 0 ppm, respectively. HPLC were obtained on a HP 1090 Liquid Chromatograph by injecting 10  $\mu\text{L}$  of a 5 ppt sample onto a polyvinylalcohol-silicagel column and eluting at 1 mL / minute using a 5 vol % THF / 95 vol % cyclohexane mobile phase and a Varex MKIII evaporative light scattering detector.

### *Synthesis of Cyclohexyl POSS-chloride [ $(c\text{-C}_6\text{H}_{11})_7\text{Si}_8\text{O}_{12}](\text{Cl})$ ].*

Under a dry nitrogen atmosphere, a 20 mL THF solution of  $\text{SiCl}_4$  (1.673g, 9.85 mmol) was slowly added to 50 mL THF solution of  $\text{Cy}_7[\text{Si}_7\text{O}_9](\text{OH})_3$  (9.130, 9.37 mmole) and  $\text{NEt}_3$  (2.942g, 29.07 mmole). After stirring overnight, the reaction was filtered to remove  $\text{HNEt}_3\text{Cl}$  (3.71 g, 26.95 mmole was isolated) and the solution evaporated to dryness. The resulting solid was extracted with THF, refiltered and the solution evacuated until crystals started to precipitate from solution. This was then added to an equivalent volume of dry  $\text{CH}_3\text{CN}$  to fully precipitate the product. After stirring for 30 minutes, a fine white precipitate was collected and dried (under nitrogen) to give a 98 % isolated yield (9.54 g, 9.22 mmole).  $^1\text{H}$  NMR (ppm): 1.74 (br, mult, 35 H); 1.24 (br, mult, 35 H); 0.78 (br, mult, 7 H).  $^{13}\text{C}\{^1\text{H}\}$  NMR (ppm): 27.45, 27.36, 26.86, 26.76, 26.59, 26.40 ( $\text{CH}_2$ ); 23.13, 23.06, 22.80 (CH).  $^{29}\text{Si}\{^1\text{H}\}$  NMR (ppm): -67.89 (s, 3 Si), -68.47(s, 3 Si), -68.53 (s, 1 Si), -89.28 (s, 1 Si-Cl). HPLC showed a single peak.

*Synthesis of Cyclopentyl POSS-chloride [(c-C<sub>5</sub>H<sub>9</sub>)<sub>7</sub>Si<sub>8</sub>O<sub>12</sub>](Cl).*

The same method used for the synthesis of the cyclohexylPOSS-chloride was followed and product was isolated in a 98 % yield. <sup>1</sup>H NMR (ppm): 1.77 (br, mult, 14 H); 1.54 (br, mult, 42 H); 1.04 (br, mult, 7 H). <sup>13</sup>C{<sup>1</sup>H} NMR (ppm): 27.29, 27.23, 27.03, 26.94; 22.22, 22.16, 21.95 (CH). <sup>29</sup>Si{<sup>1</sup>H} NMR (ppm): -65.74 (s, 3 Si), -66.32(s, 3 Si), -66.36 (s, 1 Si), -89.53 (s, 1 Si-Cl). HPLC showed a single peak.

*Synthesis of Cyclohexyl POSS-dimer [(c-C<sub>6</sub>H<sub>11</sub>)<sub>7</sub>Si<sub>8</sub>O<sub>12</sub>]<sub>2</sub>O.*

In a heavy walled glass reaction vessel under a dry nitrogen atmosphere, 0.41 ml of n-BuLi (2.5M, 1.03 mmole) was added to a well-stirred dry 10 mL THF solution of Cy<sub>7</sub>T<sub>8</sub>(OH) (1.000 g, 0.984 mmole). After stirring for 1 hour, a 10 mL THF solution of Cy<sub>7</sub>T<sub>8</sub>(Cl) (1.018 g, 0.984 mmole) was added, the reaction vessel was sealed and then heated to 60 °C overnight. The following day, the THF was removed under vacuum and the resulting white solid was extracted with ether (20 mL), filtered to remove LiCl and the filtrate precipitated into 100 mL of methanol. The product was collected by filtration and further purified by redissolving in ether and precipitating slowly via the slow addition of methanol. This product was isolated in 67% yield (1.33 g, 0. 66 mmole). <sup>1</sup>H NMR (ppm): 1.74 (br, mult, 5 H); 1.24 (br, mult, 5 H); 0.76 (br, mult, 1 H). <sup>13</sup>C{<sup>1</sup>H} NMR (ppm): 27.50, 27.46, 26.90, 26.85, 26.62, 26.43 (CH<sub>2</sub>); 23.15, 23.12, 22.82 (CH). <sup>29</sup>Si{<sup>1</sup>H} NMR (ppm): -67.67 (s, 3 Si); -68.46 (s, 3 Si); -68.49 (s, 1 Si); -109.77 (s, 1 Si). Elemental analysis found (theoretical): %C 50.12 (50.11); %H 7.88 (7.71). HPLC showed a single peak.

*Synthesis of Cyclopentyl POSS-dimer [(c-C<sub>5</sub>H<sub>9</sub>)<sub>7</sub>Si<sub>8</sub>O<sub>12</sub>]<sub>2</sub>O.*

The same method used for the synthesis of the cyclohexyl dimer was followed and product was isolated in a 65 % yield. <sup>1</sup>H NMR (ppm): 1.76 (br, mult, 14 H); 1.54 (br, mult, 42 H); 0.99 (br, mult, 7 H). <sup>13</sup>C{<sup>1</sup>H} NMR (ppm): 27.31, 27.04, 26.99 (CH<sub>2</sub>); 22.25, 22.20, 22.09 (CH). <sup>29</sup>Si{<sup>1</sup>H} NMR (ppm): -65.71 (s, 3 Si); -66.47 (s, 4 Si); -110.00 (s, 1 Si). Elemental analysis found (theoretical): %C 46.28 (46.27); %H 7.06 (6.99). HPLC showed a single peak.

*Synthesis of Cyclohexyl POSS-trimer [Cy<sub>7</sub>Si<sub>8</sub>O<sub>12</sub>]<sub>2</sub>[exo, exo-Cy<sub>8</sub>Si<sub>8</sub>O<sub>13</sub>].*

In a heavy walled glass reaction vessel under a nitrogen atmosphere, 0.75 ml of n-BuLi (2.5M, 1.88 mmole) was added to a well-stirred 10 mL THF solution of exo,exo-Cy<sub>8</sub>Si<sub>8</sub>O<sub>11</sub>(OH)<sub>2</sub> (1.000 g, 0.909 mmole). After stirring for 1 hour, a 10 mL THF solution of Cy<sub>7</sub>T<sub>8</sub>(Cl) (1.880 g, 1.818 mmole) was added, the reaction vessel was sealed and then heated to 60 °C overnight. The following day, the THF was removed under vacuum and the resulting white solid was extracted with ether (20 mL), filtered to remove LiCl and the filtrate precipitated into 100 mL of methanol. The product was collected by filtration and further purified by redissolving in ether and extracting with water, dilute HCl, water and brine solution. After drying the Et<sub>2</sub>O solution over MgSO<sub>4</sub>, the product was precipitated by slow addition to methanol. This product was isolated in 73 % yield (2.060 g, 0.665 mmole). <sup>1</sup>H NMR (ppm): 1.73 (br, mult, 5 H); 1.24 (br, mult, 5 H); 0.76 (br, mult, 1H). <sup>13</sup>C{<sup>1</sup>H} NMR (ppm): 27.59, 27.49, 26.89, 26.86, 26.60, 26.54, 26.46 (CH<sub>2</sub>); 24.06, 23.64, 23.38, 23.14, 23.08, 22.98 (CH). <sup>29</sup>Si{<sup>1</sup>H} NMR (ppm): -65.67 (s, 1 Si); -67.57 (s, 1 Si); -67.81 (s, 3 Si); -67.88 (s, 1 Si); -68.37 (s, 3 Si); -68.40 (s, 1 Si); -68.88 (s, 1 Si); -110.09 (s, 1 Si). Elemental analysis found (theoretical): %C 51.37 (51.22); %H 7.96 (7.88). HPLC showed a single peak.

Crystal Structure Analysis<sup>37-42</sup>

Single crystal X-ray diffraction data were collected on a Bruker 3-circle platform diffractometer equipped with a SMART CCD (charge coupled device) detector with the  $\chi$ -axis fixed at 54.74° and using MoK<sub>α</sub> radiation ( $\lambda = 0.71073$  Å) from a fine-focus tube. This diffractometer was equipped with an Oxford Cryostream 700 series for low temperature data collection with an error limit of +/- 0.01°C using controlled liquid nitrogen boil off. The goniometer head, equipped with a Nylon Cryoloop with a magnetic base, was then used to mount the crystals using PFPE (perfluoropolyether) oil and mounted on the magnetic goniometer. Cell constants were determined from 90 thirty-second frames at 100 K. A



complete hemisphere of data was scanned on omega ( $0.3^\circ$ ) with a run time of thirty-second per frame at a detector resolution of 512 x 512 pixels using the SMART software. A total of 2400 frames were collected in three sets and final sets of 50 frames, identical to the first 50 frames, were also collected to determine any crystal decay. The frames were then processed on a PC running on Windows NT software by using the SAINT software to give the hkl file corrected for Lp/decay. The absorption correction was performed using the SADABS program. The structures were solved by the direct method using the SHELX-90 program and refined by the least squares method on  $F^2$ , SHELXL-97 incorporated in SHELXTL Suite 6.14 for Windows XP. All non-hydrogen atoms were refined anisotropically. For the anisotropic displacement parameters, the  $U(\text{eq})$  is defined as one third of the trace of the orthogonalized  $U_{ij}$  tensor. The residual electron density around the cyclohexyl group on one of the POSS cores (Cage1- Si1-Si8) show a disorder. Both these disordered six-membered rings exhibit a chair conformation, which are located on silicon atom Si1.

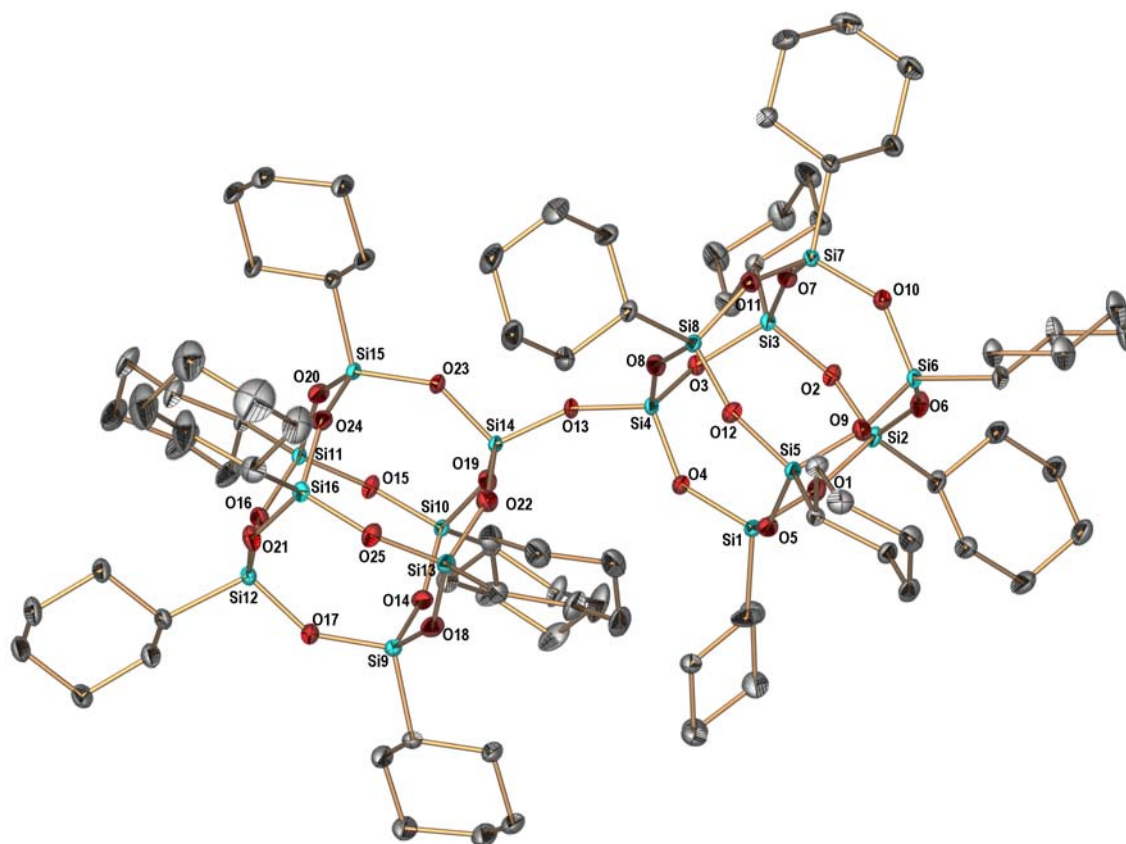


**Figure 1.** Dimer X-ray structure at 100K. Si atoms are blue, O atoms are red and carbon atoms gray. Thermal ellipsoids are shown at a 50 % probability level.

Partial occupancy refinement of the two cyclohexyl rings show a site occupancy refinement of 71 and 29%, respectively. Whereas the cyclohexyl rings on cage2 (Si9-Si16) are almost coplanar, the ones on Core1 are oriented in a more orthogonal fashion. Following this partial site occupancy refinement, no extra electron density residuals were observed.

### *Ion Mobility/Mass Spectrometry*

All experimental work on the POSS siloxanes was carried out on a home built MALDI-TOF instrument, the details of which have previously been published.<sup>22,43-46</sup> To briefly summarize, sodiated  $[\text{Cp}_7\text{T}_8]_2\text{O}.\text{Na}^+$  ions were formed in the ion source using MALDI; 2,5-dihydroxybenzoic acid (DHB) was used as the matrix and tetrahydrofuran (THF) as the solvent. Typically 50  $\mu\text{L}$  of DHB (100 mg/mL), 50  $\mu\text{L}$  of the POSS siloxane sample (1 mg/mL) and 8  $\mu\text{L}$  of NaI (saturated in THF) were applied to the sample target and dried. A nitrogen laser ( $\lambda=337$  nm, 12 mW power) was used to generate ions in a two-section (Wiley-McLaren) ion source. The ions were accelerated to 9kV for travel down a 1-meter flight tube, and detected in the reflectron mode yielding a high-resolution mass spectrum. To obtain the ion mobility, the reflectron was turned off and a linear mass gate was used for mass selection. The mass selected ions were decelerated and injected into a 20-cm long drift cell filled with  $\sim 1.5$  torr of helium gas. The ions traverse the drift cell under the influence of a weak electric field. The ion mobility cell temperature can be varied from 80K to 500K. Upon exiting the cell, the ions are again mass selected and detected as a function of time, generating an arrival time distribution (ATD). where the constant  $K$  is termed the mobility and at standard temperature  $T$  and pressure  $p$ . The arrival time can be related to the mobility via equ. 1

$$t_A = \frac{l^2}{K_o} \frac{1}{760} \frac{273}{T} \left( \frac{p}{V} \right) + t_o \quad (1)$$

where  $l$  is the cell length,  $p$  the pressure,  $V$  the voltage across the cell,  $K_o$  the reduced mobility, and  $t_o$  the time spent after exiting the cell until reaching the detector. Plotting the arrival time ( $t_A$ ) vs.  $p/V$  gives a straight line with intercept  $t_o$  and a slope proportional to  $1/K_o$ . The cross-section is then calculated from  $K_o$  using kinetic theory<sup>47</sup>

$$\sigma = \frac{3q}{16NK_o} \left( \frac{2\pi}{\mu k_b T} \right)^{1/2} \quad (2)$$

where  $q$  is the ion charge,  $N$  is the gas density in the cell,  $\mu$  the ion-He reduced mass, and  $k_b$  the Boltzmann's constant.

### *Theoretical Modeling*

We carry out molecular mechanics/molecular dynamics (MM/MD)<sup>48</sup> calculations using the AMBER 7 and 8 suites of programs to obtain low-energy structures and an annealing protocol that utilizes repeated cycles of high temperature heating, cooling and energy minimization. The annealing protocol typically heats structures to 1400K for 10ps and then cools exponentially for 30 ps to 50K before energy minimization. Cation are restrained using a built-in AMBER distance restraint so that they do not “dissociate” at high temperature. At least 100 candidate structures are employed to generate a diagnostic graph of calculated cross-sections vs. relative energy. In order to model POSS materials, we developed AMBER parameters for Si from the ab initio calculations of Sun and Rigby<sup>31,49</sup> that were originally designed to provide force field parameters for polysiloxanes. Our parameter database has been updated using recent crystal structure data<sup>50,51</sup> which give more accurate Si-O and Si-C distances and which reproduce experimental cross-sections.<sup>22,52-54</sup> We use Hyperchem<sup>55</sup> to build starting structures for AMBER and to visually inspect the calculated minimum energy structures. Charges were calculated by the standard

A modified projection model<sup>47, 56</sup> is used to calculate accurate cross-sections for systems with masses below about 1500 Daltons. For systems above about 1500 Daltons this method underestimates

the true cross-section, due to the occurrence of multiple ion-He encounters during collisions. Between 1500 and 5000 Daltons a trajectory model is utilized that incorporates a Lennard-Jones interaction potential.<sup>57</sup> It is our experience that this model can, at times, overestimate the cross-section, but usually gives more reliable values than the projection model in this size range. For larger systems the Lennard-Jones potential is replaced by a hard sphere potential that generally gives reliable results.<sup>58,59</sup> Since the siloxanes studies here have masses between 1800 and 3200 Daltons, they fall in the uncertain borderline region and hence care must be taken to ensure that consistent results are obtained.

#### *DFT Calculations*

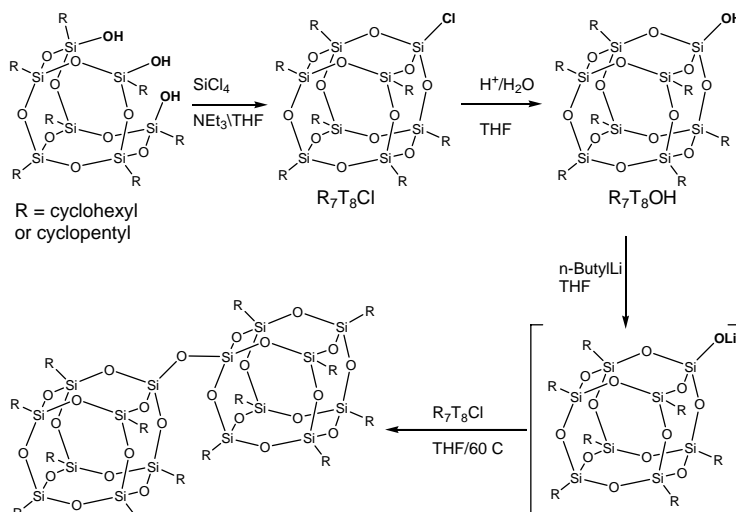
DFT calculations<sup>60</sup> were carried out using the Gaussian 03 package<sup>61</sup> of programs, using the B3LYP hybrid functional.<sup>62,63</sup> For all of the calculations reported here, the atoms silicon, oxygen, carbon and hydrogen employed the standard 6-31+G\*\* basis set.<sup>64</sup>

## Results and Discussion

### Synthesis of POSS siloxane dimers and trimer.

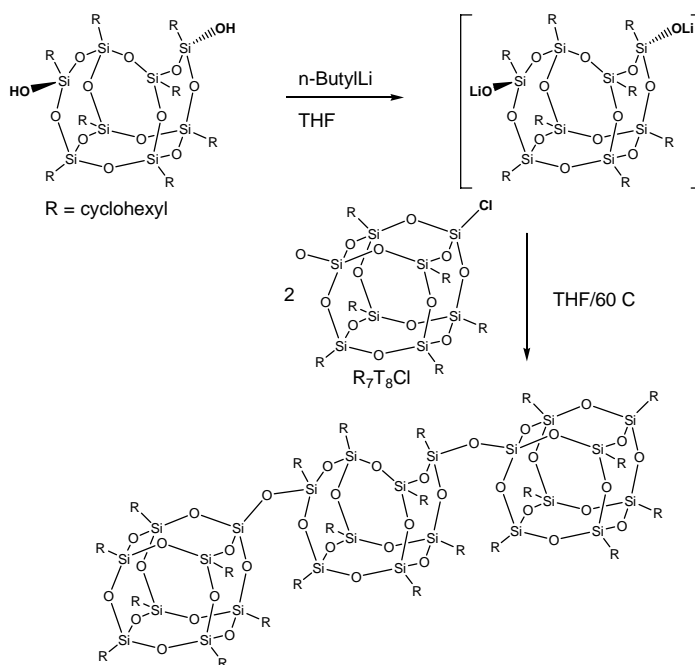
Scheme 1 shows the synthesis of the POSS dimers. POSS trisilanols are easily converted into a fully condensed  $R_7T_8Cl$  with a single Si-Cl bond in virtually quantitative yield.

These materials are slightly hydroscopic and are readily transformed into  $R_7T_8OH$  mono silanols via acidic hydrolysis in THF solution.<sup>65</sup> The monosilanols are deprotonated



**Scheme 1.** Synthesis of POSS dimers.

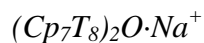
*in situ* with n-butyllithium and then reacted with another equivalent of  $R_7T_8Cl$  to generate the dimers in moderate yield. The deprotonation step is rapid, as evidenced by a small 2.5 ppm shift in the  $^{29}Si$  NMR spectroscopy as the Si-OH is converted to Si-OLi. It is worth noting that similar reactions using NEt<sub>3</sub> as the base to deprotonate the monosilanol and form the dimers was extremely slow even when heated in a sealed vessel to 170 °C for 2 days (< 50 % conversion). Better results were obtained using NaH as a base, but yields of products were low.<sup>66</sup>



**Scheme 2.** Synthesis of the cyclohexylPOSS trimer.

Scheme 2 shows the related synthesis of the POSS siloxane trimer. The cyclohexylPOSS disilanol is first deprotonated with n-butyllithium, and then heated in THF with two equivalents of cyclohexylPOSS chloride to generate the trimer in good yield

The structure of the diol is such that if the substitution chemistry at the silanols were to proceed via inversion of stereochemistry an alternative isomer could be generated. However, this is not to be expected<sup>67,68</sup> and both the NMR spectra and the MALDI data are consistent with the single isomer shown in Scheme 2.



A mass spectrum and ATD for the cyclopentyl dimer is given in Figure 2. A single peak ATD is observed (see inset figure) with a width consistent with a single conformer. The scatter plot of cross section versus relative energy for 100 structures obtained from our simulated annealing protocol is given in Figure 3. Two families of structures are obtained. The lower-energy, more compact

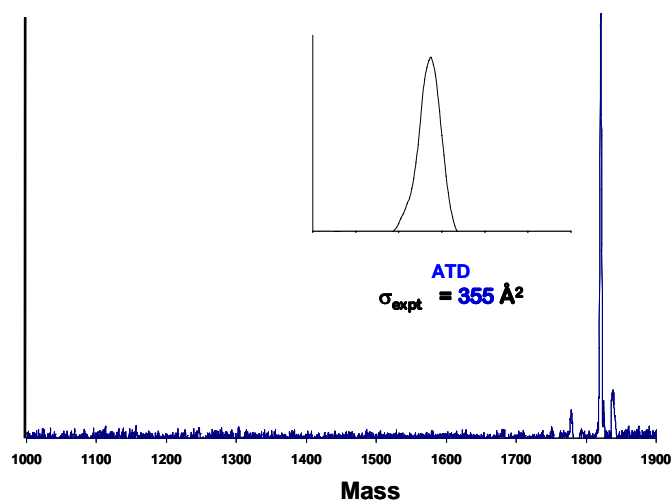


**Figure 2.** MALDI-TOF mass spectrum of  $(\text{Cp}_7\text{T}_8)_2\text{O}\cdot\text{Na}^+$  oligomers. Inset shows arrival time distributions (ATD) of  $(\text{Cp}_7\text{T}_8)_2\text{O}\cdot\text{Na}^+$  at a drift cell temperature of 300K.

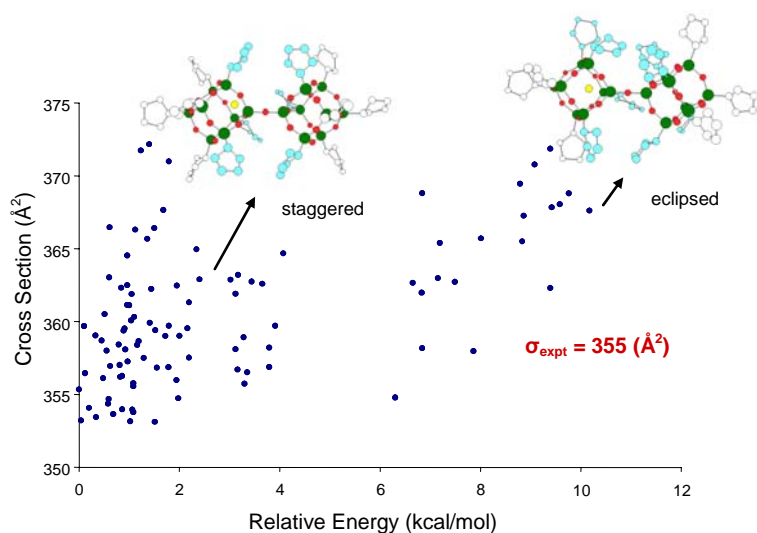


**Figure 3.**  $[\text{Cp}_7\text{T}_8]_2\text{O}\cdot\text{Na}^+$  Siloxane 2-mer Scatter Plot. Two families of structures are shown.

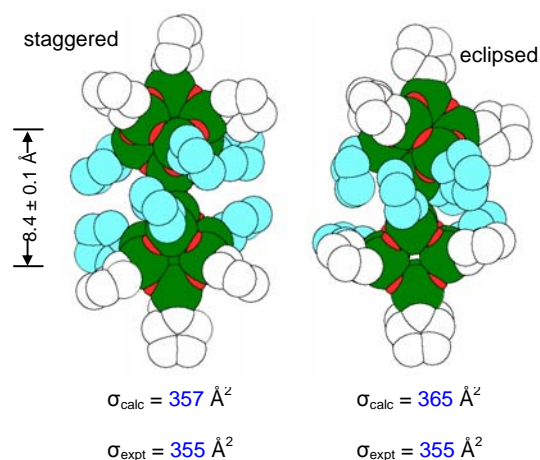
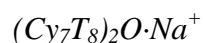


**Figure 4.** Staggered and eclipsed conformers of the cyclopentyl dimer,  $(\text{Cp}_7\text{T}_8)_2\text{O}\cdot\text{Na}^+$ . Cp = cyclopentyl groups shown in blue show which cp's are interacting.

family we label as staggered since the Cp groups on adjacent POSS cages are “staggered” with respect to each other due to a rotation of about 30% about the Si-O-Si bond connecting the two POSS cages. The higher-energy “eclipsed” form does not have this rotation, causing capping group repulsion and a small but measurable displacement of one cage relative to the other. Space filling models of the two families of structures are given in Figure 4 along with the experimental and average cross sections of the two model structures. Experiment is in excellent agreement with the staggered family cross section (0.5%) but is 3.1% smaller than the eclipsed family average cross section. For simple structures such as these, agreement between experiment and theory is consistently smaller than 2%. Hence, the staggered family of structures seems preferred, but we cannot distinguish a cross-section which would be the average of the two families. Dynamics calculations at 300K indicate these two conformations do interconvert. The fact the experimental cross-sections is in better agreement with the staggered conformation and the fact this conformation is 6 to 8 kcal lower in energy (according to AMBER) indicates the staggered conformation is either exclusively observed or is the strongly dominant conformer.

Of importance is the separation of cage centers of 8.3 to 8.5 Å shown in Figure 4. This is very near the minimum possible cage separation since the two cages are held together by a single oxygen atom and have rotated to best accommodate the capping groups. This distance will be used as a benchmark to characterize cage-cage interactions in oligomeric systems with large, more flexible backbones.



The cyclohexyl siloxane dimer, a closely related system, shows some marked differences from the cyclopentyl dimer due to

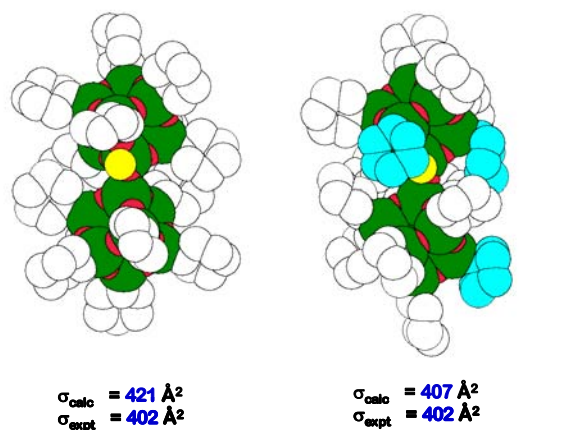


**Figure 5.** Conformers of the cyclohexyl dimer,  $(\text{Cy}_7\text{T}_8)_2\text{O}\cdot\text{Na}^+$ . Cy = cyclohexyl groups shown in white are equatorial with respect to the cage; those shown in light blue are axial (folded).

the structural features introduced by the increased isomer and conformer possibilities of the cyclohexyl group. Figure 5 shows two conformers of  $(\text{Cy}_7\text{T}_8)_2\text{O}\cdot\text{Na}^+$ . The structure on the left shows all of the Cy groups bonded to the cage silicons in equatorial chair conformation, while in the one on the right some chair conformations of the cyclohexyl group are folded with respect to the POSS cage. This R-group folding results in modeled structures which are more compact and whose cross-sections agree well with the experimental value of  $402 \text{ \AA}^2$ . ATDs were measured at low temperature to see if multiple structures could be resolved. Only a single feature consistent with a single structure (or multiple structures nearly identical in size) was observed.

A careful analysis of cyclohexyl folding raises several interesting points. If one tabulates the 100 structures formed via simulated annealing, structures with 2-4 folds very closely match the experimental cross-section while structures with less than two folds are too large. Scatter plots of cross-section vs. relative energy show the smaller structures (with increasing number of folds) aggregate in the minimum energy corner of the plots. We carried out dynamics calculations for 1 ns at 300K, shown in Figure 6. The folded and unfolded structures do not interconvert at this temperature. Dynamics carried out at 800K for the same starting structures, however, show that cross-sections immediately converge to the same value, implying that the barrier for this process is relatively small.

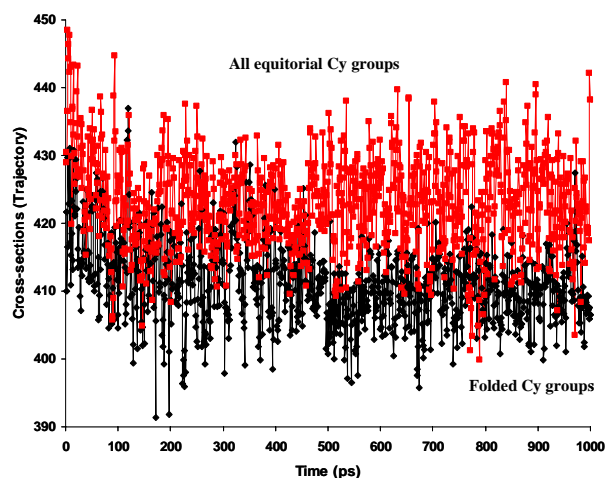


**Figure 6.**  $(\text{Cy}_7\text{T}_8)_2\text{O}\cdot\text{Na}^+$  dynamics for 1 ns at 300K. The folded (black) and unfolded (red), all equatorial Cy's, do not interconvert.

Conventional wisdom is that bulky substituents such as t-butyl groups (and POSS cages) should occupy equatorial positions when attached to a cyclohexyl ring. A DFT calculation was carried out to optimize the geometry of a POSS system with one Cy group in the equatorial position and then repeated using an axial Cy group. The two optimized structures were then used as inputs to calculate the



transition state energy for cyclohexyl axial-equatorial folding via a twisted chair conformation. The optimized structures differ in energy by less than 2 kcal/mol and that the barrier to interconversion (i.e. folding) of equatorial to axial is  $< 7.0$  kcal/mol. There are precedents for axial R-groups. For example, in cyclohexyl-HgCl, the -HgCl substituent prefers the axial position.<sup>69</sup> Since both Hg and Si have empty d-orbitals, it may be that back-bonding of ring H-atom electron density stabilizes the axial conformation or the longer Hg-C and Si-C bonds (compared to C-C) facilitates folding for steric reasons.

Even in the gas phase, intramolecular packing of Cy groups stabilizes the folded ring conformations; the cyclohexyl groups on adjacent cages are less crowded if folded in the region between the cages because of the constraint imposed by the covalent oxygen bridge in forcing the cages closer together.

To further investigate possible ring conformers, we have obtained the crystal structure of this cyclohexyl dimer at both low temperature (see Figure 1) and room temperature. The structure obtained at room temperature has very complicated unresolved disorder for the cyclohexyl groups due to chair-boat interconversion. However, at low temperature this disorder is completely resolved; all fourteen cyclohexyl groups are in the chair conformation, and only one of these chairs has two orientations (modeled with a 71:29 partial site occupancy). The distance between the cage centroids at room temperature (8.224 Å) and low temperature (8.297 Å) differs by less than 0.1 Å. Other features from the structure are typical for POSS cages and are summarized in Table 1.

The cross-section calculated using the low temperature x-ray coordinates with all Cy's equatorial in the chair conformation is 410 Å<sup>2</sup> which is slightly larger than experiment (402 Å<sup>2</sup>). Presumably the experimental sample is deposited on the sample holder with all the Cy's equatorial. It is possible that energy transferred during the MALDI process allows cyclohexyl group folding. Packing effects that sustain the equatorial Cy position in the solid are absent in the gaseous phase and an axial/equatorial mixture results.

A very low barrier to cyclohexyl chair-boat interconversion in the solid state, presumably due to crystal packing effects, was recently demonstrated in a paper containing X-ray crystal structure determinations of three different cyclohexyl<sub>8</sub>T<sub>8</sub> crystal types.<sup>70,71</sup> These crystal structures clearly exhibit stabilization of a variety of cyclohexyl group conformations for cyclohexyl<sub>8</sub>T<sub>8</sub>, depending on the conditions of crystal formation, implying these packing effects are subtle. In one structure three adjacent molecules *in the same unit cell* depict one of the POSS cages with all cyclohexyl groups equatorial in the chair conformation, another with two of the eight cyclohexyls adjacent to one another on an edge of the POSS cage in a twisted boat conformation, and the third POSS cage having two of the cyclohexyls in perfect boat conformations situated on the cube cage diagonal. This co-existence of conformations within the same crystal structure is strong evidence that the energy barriers between these structures is very low, and that slight differences in crystal packing can produce these slight differences in cyclohexyl ring conformation. Cyclohexyl groups folded axially with respect to the POSS cage are, however, not observed in these crystal structures. However, in our dimers where cages are covalently bonded together, a much stronger *intramolecular* packing effect is expected. This interpretation is consistent with minimum cage-cage center distances in the crystal structures reported by Bassindale<sup>70,71</sup> in the range of 10.2 – 11.2 Å, while the same distance in the constrained bonded structure (Figure 6) obtained from modeling are significantly smaller (8.1 – 8.4 Å). “Folding” also appears in our modeling of the cyclopentyl dimer, but folded structures (one or two cp groups) are distributed more or less randomly in our scatter plot. This folding has much less impact on the cross-section because the Cp groups are smaller. It is perhaps worth noting that in the x-ray structure of n-octyl<sub>8</sub>T<sub>8</sub>, the shortest distance between POSS cage centroids is 8.5 Å. In this near “cylindrical” molecule, the n-octyl groups are aligned on opposite sides of the cube and stretched out nearly parallel to each other, which allows the close packing of the POSS cages.<sup>71</sup>



The siloxane trimer is structurally distinct from the dimer because the central POSS unit has an open-cage *exo,exo*- $\text{Cy}_8\text{Si}_8\text{O}_{11}(\text{OH})_2$  structure (Scheme 2). During the synthesis, when the silanol hydrogens are replaced with  $\text{T}_8$  cages to form the trimer  $[\text{Cy}_7\text{T}_8\text{O}-\text{Cy}_8\text{Si}_8\text{O}_{11}-\text{OCy}_7\text{T}_8]$ , only a single isomer is observed by NMR spectroscopy. The most reasonable structure is the *exo,exo*-trimer formed by retention of stereo chemistry at the silanol silicon. The mass spectrum and ATD of the sodiated trimer are shown in Figure 7. The ATD

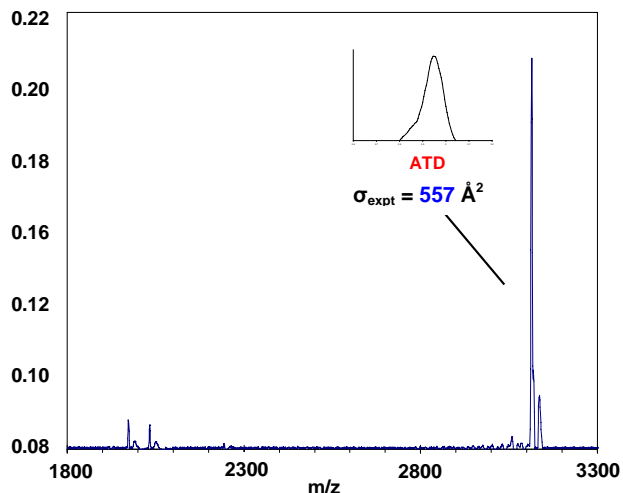


**Figure 7.** Mass spectrum and ATD (insert) for  $[\text{Cy}_7\text{T}_8\text{O}-\text{Cy}_8\text{Si}_8\text{O}_{11}-\text{OCy}_7\text{T}_8]\cdot\text{Na}^+$  trimer.

has only a single peak with a width consistent with a single family of structures or unresolved multiple families since several isomers are possible. Scatter plots were calculated after modeling the three possible isomers, all of which have cross-sections within 1% of  $\sim 570 \text{ \AA}^2$  for the lowest energy conformations. Our interpretation is similar to that for the cyclohexyl dimer above. More compact higher energy structures are obtained (average  $\sigma_{\text{calc}} = 557 \text{ \AA}^2$ ) for each isomer if several of the

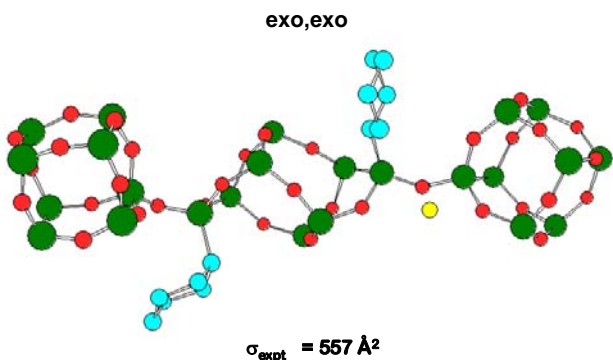


**Figure 8.** *Exo,exo*- isomer of the  $[\text{Cy}_7\text{T}_8\text{O}-\text{Cy}_8\text{Si}_8\text{O}_{11}-\text{OCy}_7\text{T}_8]\cdot\text{Na}^+$  trimer, showing folded and unfolded  $\text{Cy} =$  cyclohexyl groups in blue. H atoms and most of the  $\text{Cy}$  groups are omitted for clarity.

Figure 8 where all cyclohexyl-groups except those on the silicon defining the “endo” or “exo” stereochemistry have been deleted for clarity; the  $\text{Cy}$  groups shown in this figure also illustrate the

cyclohexyl groups are allowed to fold into an axial position as in the dimer. These structures arise naturally in the annealing procedure where the heating is at 1400K and subsequent cooling freezes out folded  $\text{Cy}$  groups. Average calculated cross-sections are in excellent agreement with experiment ( $\sigma_{\text{expt}} = 557 \text{ \AA}^2$ ). The *exo-exo* isomer is shown in

unfolded equatorial (on right) and the folded axial (on left, pointing down) orientations. The stereochemistry of the diol precursor in the synthesis of the trimer predicts the exo-exo isomer but we cannot prove this structure is obtained in our experiment since all the isomers are virtually identical in size. Molecular dynamics calculations indicate that while exo-exo folded structures do not interconvert at 300 K (they do at 1400K), and since they overlap in cross-section, we are most likely observing a weighted average of exo-exo folded structures in the ATD. Since the barrier is small, the activation energy for conversion is presumably supplied in the MALDI process.

In summary, we have used ion mobility mass spectrometry to measure the cross-sections of the sodiated dimers  $(\text{Cy}_7\text{T}_8)_2\text{O}\cdot\text{Na}^+$  and  $(\text{Cp}_7\text{T}_8)_2\text{O}\cdot\text{Na}^+$ , and the trimer ion  $[\text{Cy}_7\text{T}_8\text{O}-\text{Cy}_8\text{Si}_8\text{O}_{11}-\text{OCy}_7\text{T}_8]\text{Na}^+$ . Structures obtained by molecular modeling agree with experiment within ~2%. The cyclopentyl dimer shows a low energy staggered structure determined primarily by non-bonded interactions of the cyclopentyl capping groups. The cyclohexyl dimer structure is consistent with several cyclohexyl groups interconverting rapidly between axial and equatorial conformations. A low temperature crystal structure shows all cyclohexyl groups frozen out in equatorial conformations. The capping cyclohexyl groups disorder due to thermal motion. The trimer structure is consistent with the exo-exo isomer, exclusively produced by retention of stereochemistry from the exo- $\text{Cy}_8\text{T}_8(\text{OH})_2$  starting material. The cross-section agrees with experiment if the same sort of rapid interconversion of folded and unfolded cyclohexyl groups occurs as in the corresponding dimer.

Larger siloxane oligomers and siloxane copolymers are being synthesized by the group at Edwards AFB. We are confident we will be able to analyze them and distinguish between linear and branched structures. Siloxanes from the trimer are readily cationized by  $\text{Na}^+$  due to the open nature of the central unit, allowing multiple coordination of the cationized metal ion, but with minimum influence on oligomer cross-section.

## ACKNOWLEDGMENT

The Air Force Office of Scientific Research under grant F49620-03-1-0046 is gratefully acknowledged for support of this work. We also thank the NAS/NRC Senior Associateship Program for fellowship support of S.E.A.

## REFERENCES

1. Voronkov, M. G.; Lavrentyev, V. I. *Top. Curr. Chem.* **1982**, *102*, 199-236.
2. Agaskar, P. A. *Inorg. Chem.* **1991**, *30*, 2707-2708.
3. Agaskar, P. A.; Klemperer, W. G. *Inorg. Chim. Acta* **1995**, *229*, 355-364.
4. Baney, R. H.; Itoh, M.; Sakakibara, A.; Suzuki, T. *Chem. Rev.*, **1995**, *92*, 1409-1430.
5. Lichtenhan, J. D. *Comments Inorg. Chem.*, **1995**, *17*, 115-130.
6. Lichtenhan, J. D. in *Polymeric Materials Encyclopedia*, J. C. Salamore (ed.) CRC Press, NY, **1996** 7769-7778.
7. Li, G. Z.; Wang, L. C.; Ni, H. L.; Pittman, C. U. *J. Inorg. Organomet. Polym.*, **2001**, *11* 123-154.
8. Phillips, S. H.; Haddad, T. S.; Tomczak, S. J. *Curr. Opin. Sol. State Mat. Sci.*, **2004**, *8*, 21-29.
9. Li, G. Z.; Pittman, C. U., Chapter 5 in *Macromolecules Containing Metals and Metal-like Elements*. Vol. 5 Group IVA Polymers, Abd El Aziz, A.S.; Carraher, C.E.; Pittman, C.U.; Zeldin, M., Editors, John Wiley & Sons, Hoboken, NJ, 2005, pp 79-131.
10. Lichtenhan, J. D.; Otonari, Y. A.; Carr, M. J. *Macromolecules* **1995**, *28*, 8435-8437.
11. Jeon, H. G.; Mather, P. T.; Haddad, T. S. *Polym. Int.* **2000**, *49*, 453-457.

12. Haddad, T. S.; Viers, B. D.; Phillips, S. H. *J. Inorg. Organomet. Polym.*, **2002**, *11* 155-164.
13. Lichtenhan, J. D.; Vu, N. Q.; Carter, J. A. ; Gilman, J. W. ; Feher, F. J. *Macromolecules*, **1993**, *26*, 2141-2142.
14. Byoung-Suhk K.; Mather, P. T. *Macromolecules*, **2002**, *35*, 8378-8384.
15. Fu, B. X.; Lee, A. ; Haddad, T. S. *Macromolecules*, **2004**, *37*, 5211-5218.
16. Constable, G. S.; Lesser, A. J. ; Coughlin, E. B. *Macromolecules*, **2004**, *37*, 1276-1282.
17. Pittman, C. U.; Li, G.; Ni, H., *Macromol. Symp.*, **2003**, *196*, 301-325.
18. Huang, J.; He, C.; Xiao, Y.; Mya, K. Y.; Dai, J.; Siow, Y. P. *Polymer*, **2003**, *44*, 4491-4499.
19. Kopesky, E. T.; Haddad, T. S.; Cohen, R. E.; McKinley, G. H. *Macromolecules*, **2004**, *37*, 8992-9004.
20. Zheng, L.; Hong, S.; Cardoen, G.; Burgaz, E.; Gido, S. P.; Coughlin, E. B. *Macromolecules*, **2004**, *37*, 8606-8611.
21. Capaldi, F. M.; Rutledge, G. C.; Boyce, M. C. *Macromolecules*, **2005**, *38*, 6700-6709.
22. Anderson, S. E.; Mitchell, C.; Bowers, M. T.; and T. S. Haddad, *Chem. Mater.*, **2005**, *17*, 2537-2545.
23. a) Lichtenhan, J. D.; Vu, N. Q.; Carter, J. A.; Gilman, J. W.; Feher, F. J. *Macromolecules*, **1993**, *26*, 2141-2142. b) Mantz, R. A.; Jones, P. F.; Chaffee, K. P.; Lichtenhan, J. D.; Gilman, J. W.; Ismail, I. M. K.; Burmeister, M. J. *Chem. Mater.* **1996**, *8*, 1250-1259. c) Shockey, E. G.; Bolf, A. G.; Jones, P. F.; Schwab, J. J.; Chaffee, K. P.; Haddad, T. S.; Lichtenhan, J. D. *J. Appl. Orgmet. Chem.* **1999**, *13*, 311-327. d) Lichtenhan, J. D.; Mantz, R. A.; Jones, P. F.; Carr, M. J. *Polym. Prepr.* **1994**, *35(1)*, 523-524. e) Shockey, E.; Jones, P. F.; Chaffee, K. P.; Lichtenhan, J. D. *Polym. Prepr.* **1995**, *36(1)*, 391-392. f) Haddad, T. S.; Oviatt, H. W.;

- Schwab, J. J.; Mather, P. T.; Chaffee, K. P.; Lichtenhan, J. D. *Polym. Prepr.* **1998**, *39*(1), 611-612. g) Haddad, T. S.; Stapleton, R. A.; Jeon, H. G.; Mather, P. T. ; Lichtenhan, J. D.; Phillips, S. *Polym. Prepr.* **1999**, *40*(1), 496-497. h) Haddad, T. S.; Lee, A.; Phillips, S. H. *Polym. Prepr.* **2001**, *42*(1), 88-89.
24. Pan, G.; Mark, J. E.; Schaefer, D. W. *J. Appl. Polym. Sci., B: Poly. Phys.* **2003**, *41*, 3314-3323.
25. Isayeva, I. S.; Kennedy, J. P. *Polym. Mater.: Sci. Eng.* **2003**, *89*, 645-646.
26. Chan, E. R.; Zhang, X.; Lee, C-Y.; Neurock, M.; Glotzer, S. C. *Macromolecules*, **2005**, *38*, 6168-6180
27. Striolo, A.; McCabe, C.; Cummings, P. T. *J. Phys. Chem. B*, **2005**, *109*, 14300-14307
28. (a) Bahar, I.; Zuniga, I.; Dodge, R.; Mattice, W. L.; *Macromolecules*, **1991**, *24*, 2986-2992.
- (b) Bahar, I.; Zuniga, I.; Dodge, R.; Mattice, W. L.; *Macromolecules*, **1991**, *24*, 2983-2998.
- (c) Neuberger, N.; Bahar, I.; Mattice, W. L.; *Macromolecules*, **1992**, *25*, 2447-2454.
29. Bahar, I.; Neuberger, N.; Mattice, W. L.; *Macromolecules*, **1992**, *25*, 4619-4625.
30. Patel, R. D. and Mark, J.E., *Comput. Theor. Polym. Sci.*, **2000**, *10*, 189-195.
31. Sun H.; Rigby, D. *Spectrochim. Acta*, **1997**, *A 53*, 1301-1323.
32. Xiang, K.H.; Pandey, R.; Pernisz, U. C.; and Freeman, C., *J. Phys. Chem. B*, **1998**, *102*, 8704-8711.
33. Wichman, D.; and Jug, K., *J. Phys. Chem. B*, **1999**, *103*, 10087-10091.
34. Wichman, D.; and Jug, K., *J. Comput. Chem.*, **2000**, *21*, 1549-1553.
35. Franz, R.; Kandalam, A. K.; Pandey, R.; Pernisz, U. C., *J. Phys. Chem. B*, **2002**, *106*, 1709-1713.

36. Feher, F. J.; Newman, D. A.; Walzer, J. F., *J. Am. Chem. Soc.*, **1989**, *111*, 1741-1748.
37. SMART V 5.631 Software for the CCD Detector System, Bruker AXS, Madison, WI, **2003**.
38. SAINT PLUS V 6.45 Software for the CCD Detector System, Bruker AXS, Madison, WI, **2003**.
39. SADABS, Program for absorption correction for area detectors, Version 2.01, Bruker AXS, Madison, WI, **2002**.
40. Sheldrick, G. M., SHELXS-90, Program for the Solution of Crystal Structure, University of Göttingen, Germany, **1990**.
41. Sheldrick, G. M., SHELXL-97, Program for the Refinement of Crystal Structure, University of Göttingen, Germany, **1997**.
42. SHELXTL 6.14 for Windows, Program library for Structure Solution and Molecular Graphics, Bruker AXS, Madison, WI, **2003**.
43. Baker, E.S.; Gidden, J.; Fee, D.P.; Kemper, P.R.; Anderson, S.E.; Bowers, M.T., *Int. J. Mass Spectrom.*, **2003**, *227*, 205-216.
44. Bowers, M.T.; Kemper, P.R.; von Helden, G.; van Koppen, P.A.M., *Science*, **1993**, *260*, 1446-1451.
45. Bowers, M.T. *Accts. Chem. Res.*, **1994**, *27*, 324-332.
46. von Helden, G.; Batka, J.T.; Carlot D.; Bowers, M.T. *J. Am. Soc. Mass Spectrom.*, **1997**, *8*, 275-282; Wyttenbach, T.; Witt, M.; Bowers, M.T. *J. Am. Chem. Soc.*, **2000**, *122*, 3458-3464.
47. McDaniel E.W.; Mason, E.A. *The Mobility and Diffusion of Ions in Gases*, Wiley, NY, **1973**.
48. (a) Kollman, P.A.; *et. al.*, AMBER6, University of California at San Francisco, **1999**.



- (b) D.A. Case, D. A.; Darden, T.A.; Cheatham, III, T.E.; Simmerling, C.L. ; Wang, J. ; Duke, R.E. ; Luo, R., ; Merz, K.M. ; Wang, B. ; Pearlman, D.A. ; Crowley, M. ; Brozell, S.; Tsui, V.; Gohlke, H.; Mongan, J.; Hornak, V.; Cui, G.; Beroza, P.; Schafmeister, C.; Caldwell, J.W.; Ross, W.S.; and Kollman, P.A., AMBER 8, University of California, San Francisco, **2004**.
49. Sun, H. *Macromolecules*, **1995**, 28, 701-712.
  50. Bassindale, A.R.; Pourny, M.; Taylor, P.G.; Hursthouse, M.B.; Light, M.E. *Angew. Chem., Int. Ed.*, **2003**, 42, 3488-3490.
  51. Itami, Y.; Marciniak, B.; Kubicki, M. *Chem. Eur. J.*, **2004**, 10, 1239-1248.
  52. Gidden, J. ; Kemper, P.R.; Shammel, E. ; Fee, D.P.; Anderson, S.E.; and Bowers, M.T., *Int. J. Mass Spectrom.*, **2003** 63, 222-.
  53. Baker, E.S. ; Gidden, J.; Fee, D. P.; Kemper, P. R.; Anderson, S. E.; and Bowers, M. T., *Int. J. Mass Spectrom.* **2003**, 205, 227-.
  54. Baker, E. S.; Gidden, J.; Anderson, S. E.; Haddad, T. S.; and Bowers, M.T., *Nano Lett.*, **2004**, 4, 779-.
  55. HyperChem(TM) Professional 7.5, Hypercube, Inc., 1115 NW 4th Street, Gainesville, Florida 32601, USA
  56. von Helden, G.; Wytenbach, T.; Bowers, M.T. *Int. J. Mass Spectrom. Ion Proc.*, **1995**, 146/147, 349-364.
  57. Melsch, M.F.; Hunter, J.M.; Svartsburg, A.A.; Schatz, G.C.; and Jarrold, M.F. *J. Phys. Chem.*, **1996**, 100, 16082-16086.
  58. Shvartsburg, A.A.; Jarrold, M.F. *Chem. Phys. Lett.*, **1996**, 261, 86-91.
  59. See, for example, Bernstein, S.L. ; Wytenbach, T. ; Baumketner, A. ; Shea, J-E. ; Betan, G. ; Teplow, D.B.; Bowers, M.T., *J. Am. Chem. Soc.*, **2005**, 127, 2075-2084.

60. (a) Hohenberg, P.; Kohn, W. ; *Phys. Rev. B* , **1964**, *136*, 864; (b) Kohn, W.; Sham, L.J., *Phys. Rev.* **1965**, *140*, 1133.
61. Stephens, P.J.; Devlin, F.J.; Chabalowski, C.F.; and Frisch, M.J., *J. Phys. Chem.*, **1994**, *98*, 11623.
62. (a) Becke, A.D., *J. Chem. Phys.*, **1993**, *98*, 5648; (b) Becke, A.D., *Phys Rev A*, **1988**, *38*, 3098.
63. Gaussian 03, Revision B.04, Frisch, M. J.; Trucks, G. W.; Schlegel, H. B.; Scuseria, G. E.; Robb, M. A.; Cheeseman, J. R.; Montgomery, Jr., J. A.; Vreven, T.; Kudin, K. N.; Burant, J. C.; Millam, J. M.; Iyengar, S. S.; Tomasi, J.; Barone, V.; Mennucci, B.; Cossi, M.; Scalmani, G.; Rega, N.; Petersson, G. A.; Nakatsuji, H.; Hada, M.; Ehara, M.; Toyota, K.; Fukuda, R.; Hasegawa, J.; Ishida, M.; Nakajima, T.; Honda, Y.; Kitao, O.; Nakai, H.; Klene, M.; Li, X.; J. E. Knox, J. E.; Hratchian, H. P.; Cross, J. B.; Adamo, C.; Jaramillo, J.; Gomperts, R.; Stratmann, R. E.; Yazyev, O.; Austin, A. J.; Cammi, R.; Pomelli, C.; Ochterski, J. W.; Ayala, P. Y.; Morokuma, K.; Voth, G. A.; Salvador, P.; Dannenberg, J. J.; Zakrzewski, V. G.; Dapprich, S.; Daniels, A. D.; Strain, M. C.; Farkas, O.; Malick, D. K.; Rabuck, A. D.; Raghavachari, K.; Foresman, J. B.; Ortiz, J. V.; Cui, Q.; Baboul, A. G.; Clifford, S.; Cioslowski, J.; Stefanov, B. B.; Liu, G.; Liashenko, A.; Piskorz, P.; Komaromi, I.; Martin, R. L.; Fox, D. J.; Keith, T.; Al-Laham, M. A.; Peng, C. Y.; Nanayakkara, A.; Challacombe, M.; Gill, P. M. W.; Johnson, B.; Chen, W.; Wong, M. W.; Gonzalez, C.; Pople, J. A., Gaussian, Inc., Pittsburgh PA, **2003**.
64. (a) Francl, M.M.; Pietro, W.J.; Hehre, W.J.; Binkley, J.S.; Gordon, M.S.; Defrees, D.J.; Pople, J.A., *J. Chem. Phys.* **1982**, *77*, 3654; (b) Clark, T.; Chandrasekhar, J.; Spitznagel, G.W.; Schleyer, P.V., *J. Comput. Chem.*, **1983**, *4*, 294; (c) Krishnan, R.; Binkley, J.S.; Seeger, R.;

- Pople, J.A., *J. Chem. Phys.*, **1980**, 72, 650; (d) Gill, P.M.W.; Johnson, B.G.; Pople, J.A.; Frisch, M.J., *Chem. Phys. Lett.*, **1992**, 197, 499.
65. Duchateau, R.; Cremer, U.; Harmsen, R. J.; Mohamud, S. I.; Abbenhuis, H. C. L.; van Santen, R. A.; Meetsma, A.; Thiele, S. K.-H.; van Tol, M. F. H.; Kranenburg, M., *Organometallics*, **1999**, 18, 5447-5459.
66. Dr. Joe Schwab: Unpublished results.
67. Feher, F. J.; Soulivong, D.; Eklund, A. G. *Chem. Comm.* 1998, 399-400;
68. Feher, F. J.; Soulivong, D.; Nguyen, F. *Chem. Comm.* 1998, 1279-1280.}
69. Smith, M.B.; and March, J, *Advanced Organic Chemistry* (5<sup>th</sup> ed.) , Wiley-Interscience, New York, p.172-175.
70. Bassindale, A.R.; Liu, Z.; MacKinnon, I. A. ; Taylor, P. G.; Yang, Y. ; Light, M.E. ; Horton, P. N. ; Hursthouse, M.B.; *Dalton Trans.*, **2003**, 2945-2949.
71. Bassindale, A.R.; Chen, H. ; Liu, Z.; MacKinnon, I. A. ; Parker, D. J. ; Taylor, P. G.; Yang, Y. ; Light, M.E. ; Horton, P. N. ; Hursthouse, M.B.; *J. Organomet. Chem.*, **2004**, 689, 3287-3300.

**Table 1.** Summary of metrical parameters from the X-ray crystal structure of (Cy<sub>7</sub>T<sub>8</sub>)<sub>2</sub>O obtained at -173 °C.

<b>X-ray Crystal Structure Parameter</b>	<b>Average Value</b>	<b>Range of values</b>
Si-O Bond Length in Cage	1.620 Å	1.606 – 1.636 Å
Si-O Bond Length in Siloxane Bridge	1.602 Å	1.602 – 1.602 Å
Si-C Bond Length in Cage	1.848 Å	1.837 – 1.854 Å
O-Si-O Bond Angle in Cage	109.04°	107.48° - 111.04°
O-Si-O Bond Angle in Siloxane Bridge	108.89°	107.53°- 110.89°
Si-O-Si Bond Angle in Cage	148.75 °	137.94°- 168.12°
Si-O-Si Bond Angle in Siloxane Bridge	152.39°	152.39°- 152.39°

